Digital Compensation of I/Q Imbalance Effects in Space-Time Coded Transmit Diversity Systems

Yaning Zou, *Student Member, IEEE*, Mikko Valkama, *Member, IEEE*, and Markku Renfors, *Fellow, IEEE*

***Abstract*—Space-time coded wireless transmission techniques with multiple transmit and receive antennas can provide considerable increases in both the link quality as well as link capacity when compared to ordinary single-antenna techniques. However, multiantenna transmission basically calls for multiple parallel radio implementations, and the resulting link performance is found to be very sensitive to the possible nonidealities of the individual analog radio front-ends. One important practical example is the so-called I/Q imbalance problem related to the amplitude and phase matching of the I/Q branches of the transmitters and receivers. In this paper, we analyze the I/Q imbalance effects in space-time coded transmit diversity system context, in terms of the resulting signal-to-interference ratio as a function of the imbalance properties, assuming the individual transmitter and receiver analog front-ends are based on the so-called direct-conversion radio architecture. The obtained results indicate that the I/Q imbalance effect is fundamentally more challenging in the multiantenna context compared to traditional single-antenna systems. In addition, two digital compensation methods are proposed for combating the resulting signal distortion on the receiver side. The first approach is based on algebraic properties of the derived signal models combined with proper pilot data, while the second one is blind, stemming from the blind signal separation principles. The resulting link-level performance of the proposed algorithms is evaluated using extensive computer simulations. Based on the obtained results, the I/Q imbalance effects can be efficiently compensated using the proposed techniques, the resulting link performance being practically identical to that of the ideal perfectly matched reference case. Furthermore, the proposed methods are also shown to correct for channel estimation errors, in addition to I/Q impairments, and are also reasonably robust against residual carrier offsets.**

***Index Terms*—Complex signals and systems, digital radios, direct-conversion transceivers, I/Q imbalance, MIMO systems, signal separation, space-time coding, transmit diversity.**

I. Introduction

THE growing demands for various multimedia and personal wireless communications services call for considerable increase in the supported spectral efficiencies in future wireless systems. The so-called beyond 3G (B3G) or 4G concepts form a good example within the emerging cellular networks, where spectral efficiencies in the order of 10 b/s/Hz are commonly stated as a driving working assumption, see, e.g., [1] and [2], and the references therein. Together with the actual waveform studies targeting for more efficient modulation techniques, one key ingredient is the introduction of multiple transmit and receive antennas, leading to the so-called multiple-input multiple-output (MIMO) system concepts [1], [3], [4]. Another important aspect in this context, in addition to increased data rates, is that the use of multiple antennas offers the possibility of increasing the link quality through the obtained spatial diversity [3]–[5]. This is already part of the current 3G UMTS standard [6], under the acronym space-time transmit diversity (STTD).

Besides the system capacity and link quality issues, one crucial aspect in the evolution of wireless systems is the design and implementation of the needed user terminal equipment, and especially the radio transceivers in them. The terminal design is being more and more dictated by the increasing needs and push towards flexible and software configurable transceiver structures being able to operate over multiple frequency bands and supporting different type waveforms and different radio access technologies used in the currently existing and also emerging wireless systems [7]–[11]. The terms *multimode*, *multiband*, or *multistandard* radio are commonly used in this context. In addition to the flexibility aspects, the terminal power consumption and implementation costs and size are still expected to be kept at reasonable levels.

One of the key ingredients in building compact yet flexible radios is the efficient use of digital signal processing (DSP), combined with innovative thinking at the radio architecture layer [7], [9]–[11]. The current trend in this context is to simplify the analog front-end stages, resulting in the so-called direct-conversion and low-IF type transceiver topologies [12]–[16]. Even though rather simple in theory, these architectures are however sensitive to many nonidealities in the (remaining) analog front-end sections, arising from the fundamental physical limitations, like process variations, of the used circuit technologies. One good example is the so-called I/Q imbalance problem (see, e.g., [11], [12], [16]–[22]), stemming from the unavoidable differences in the amplitudes and phases of the physical analog I and Q signal paths. In general, with wideband modulated communication waveforms and high-order symbol alphabets, these nonidealities have a big impact on the demodulated signal quality and can easily degrade the whole transceiver operation, if not taken properly into account. The use of multiple transmit and/or receive antennas is then of major concern also in this context since multiantenna techniques basically call for multiple parallel radio front-ends, resulting in even tighter requirements

Manuscript received September 1, 2006; revised October 22, 2007. The associate editor coordinating the review of this manuscript and approving it for publication was Prof. John J. Shynk. This work was supported by the Academy of Finland (under the project 116423, "Understanding and Mitigation of Analog RF Impairments in Multiantenna Transmission Systems"), the Technology Industries of the Finland Centennial Foundation, the Finnish Graduate School TISE, Elisa HPY Foundation, and the Nokia Foundation.

The authors are with the Institute of Communications Engineering, Tampere University of Technology, FIN-33101 Tampere, Finland (e-mail: yaning.zou@tut.fi; mikko.e.valkama@tut.fi; markku.renfors@tut.fi).

Color versions of one or more of the figures in this paper are available online at http://ieeexplore.ieee.org.

Digital Object Identifier 10.1109/TSP.2007.916132

for the size and cost of the individual radio implementations. Thus, in general, understanding and mitigating the analog front-end nonidealities is of big importance in implementing future wideband multiantenna terminals.

Building understanding of the effects of analog front-end nonidealities in multiantenna systems is also the central theme in this paper, with emphasis on I/Q imbalance effects in space-time coded (STC) MIMO systems. These issues have started to receive some interest in the recent literature of the field. Some preliminary results related to signal modeling have been presented by the authors in [23] which forms the starting point for this paper. The studies reported in [24]–[29], in turn, focus on MIMO-OFDM type transmission schemes where the I/Q imbalance, when viewed from the subcarrier signals point of view, corresponds to certain type mirror-carrier interference. Then some compensation techniques utilizing OFDM pilot carriers or known preamble to suppress this interference are proposed in [25]–[27], [29]. Also the work in [28] results in novel receiver structures being able to efficiently combat I/Q mismatch effects in MIMO-OFDM type systems assuming known imbalance properties, but leaves the question of imbalance estimation open. The space-time coding aspects are touched shortly in [28], but the resulting signal degradation is not addressed analytically. Also the focus in [28] is solely on the receiver imbalance properties.

In this paper, we focus on linearly modulated space-time coded diversity transmission schemes and the I/Q imbalance effects in them. More specifically, we analyze the I/Q imbalance effects in the so-called Alamouti transmit diversity scheme [5] with two transmit antennas and M receiver antennas, assuming the direct-conversion radio architecture is used in the individual front-end implementations. I/Q imbalance effects on both the transmitter and receiver sides are taken into account. It will be shown that the I/Q imbalance problem is fundamentally different and more challenging due to the use of multiple antennas and space-time coding, when compared to ordinary single-antenna direct-conversion case. Similar conclusion is drawn also in [28], with focus only on the receiver aspects. Another key difference is that the resulting signal degradation is addressed here analytically. Closed-form analytical results for the resulting signal-to-interference ratio (SIR) are derived, forming a solid theoretical background for fully appreciating the imbalance effect in any STC/MIMO context. Furthermore, based on the derived signal models, some novel baseband DSP based techniques are also proposed to mitigate or compensate for the dominant I/Q imbalance effects on the receiver side. Here, the focus is on the total system output signals instead of the individual front-end signals. Both training/pilot signal based as well as blind compensation techniques are presented, and their performance is analyzed using extensive computer simulations. Based on the obtained results, I/Q imbalance can be efficiently removed using the proposed techniques, the resulting performance being virtually identical to that of the perfectly balanced reference system.

The organization of the paper is as follows. The essential I/Q signal and system models are presented first in Section II. Then in Section III, two novel approaches for imbalance compensation are proposed, after which some distortion and performance analysis results are presented in Section IV. Section V presents the computer simulation results, and conclusions are finally drawn in Section VI.

II. I/Q Signal and System Models

A. Mathematical Notations and Preliminaries

Throughout the text, unless otherwise mentioned explicitly, all the signals are assumed to be complex-valued, wide-sense stationary (WSS) random signals with zero mean. The so-called I/Q notation of the form $x = x_I + jx_Q$ is commonly deployed for any complex-valued quantity x, where x_I and x_Q denote the corresponding real and imaginary parts, i.e., $\mathrm{Re}[x] = x_I$ and $\mathrm{Im}[x] = x_Q$. Statistical expectation and complex-conjugation are denoted by $E[\cdot]$ and $(\cdot)^*$, respectively. We also assume that the complex random signals and random quantities at hand are, under perfect I/Q balance, circular (see, e.g., [30]), meaning basically that the I and Q components are uncorrelated and have equal variance. For a circular random signal $x(t)$, this also implies that $E[x^2(t)] = 0$ [30].

B. I/Q Mismatch Models

Physically the amplitude and phase mismatches between the transceiver I and Q signal branches stem from the relative differences between all the analog components of the I/Q front-end [7]–[16]. On the transmitter side, this includes the actual I/Q upconversion stage as well as the I and Q branch filters and D/A converters. On the receiver side, in turn, the I/Q downconversion as well as the I and Q branch filtering, amplification, and sampling stages contribute to the effective I/Q imbalance. For modeling purposes, we refer all the mismatches to the I/Q up- and downconversion stages, which is rather typical in the literature in this context, see, e.g., [11], [13], [15], [18], [22], and [24]–[28] in which the focus is mostly on the receiver issues. Taking both the transmitter and receiver imbalances into account, we write the corresponding complex local oscillator (LO) signals as

$$\begin{aligned} x_{\mathrm{LO}}^{\mathrm{TX}}(t) &= \cos(\omega_{\mathrm{LO}}t) + jg_{\mathrm{TX}}\sin(\omega_{\mathrm{LO}}t + \phi_{\mathrm{TX}}) \\ &= K_{1,\mathrm{TX}}\exp(j\omega_{\mathrm{LO}}t) + K_{2,\mathrm{TX}}\exp(-j\omega_{\mathrm{LO}}t) \qquad (1) \\ x_{\mathrm{LO}}^{\mathrm{RX}}(t) &= \cos(\omega_{\mathrm{LO}}t) - jg_{\mathrm{RX}}\sin(\omega_{\mathrm{LO}}t + \phi_{\mathrm{RX}}) \\ &= K_{1,\mathrm{RX}}\exp(-j\omega_{\mathrm{LO}}t) + K_{2,\mathrm{RX}}\exp(j\omega_{\mathrm{LO}}t) \qquad (2) \end{aligned}$$

where $\omega_{\mathrm{LO}} = 2\pi f_{\mathrm{LO}}$, $\{g_{\mathrm{TX}}, \phi_{\mathrm{TX}}\}$ and $\{g_{\mathrm{RX}}, \phi_{\mathrm{RX}}\}$ represent the total effective amplitude and phase imbalances of the transmitter (TX) and the receiver (RX), respectively, and the coefficients $K_{1,\mathrm{TX}}$, $K_{2,\mathrm{TX}}$, $K_{1,\mathrm{RX}}$, and $K_{2,\mathrm{RX}}$ are of the form $K_{1,\mathrm{TX}} = (1 + g_{\mathrm{TX}}e^{j\phi_{\mathrm{TX}}})/2$, $K_{2,\mathrm{TX}} = (1 - g_{\mathrm{TX}}e^{-j\phi_{\mathrm{TX}}})/2$, $K_{1,\mathrm{RX}} = (1+g_{\mathrm{RX}}e^{-j\phi_{\mathrm{RX}}})/2$ and $K_{2,\mathrm{RX}} = (1-g_{\mathrm{RX}}e^{j\phi_{\mathrm{RX}}})/2$. Notice that the above impairment models assume frequency-independent I/Q imbalances within the signal band. This is a rather typical assumption in this context, and can be safely assumed for relatively narrowband signals [13], [28]. From the individual transmitter and receiver point of views, the above I/Q imbalance models correspond to the following transformations of the effective baseband equivalent signals given by

$$z_{\mathrm{TX}}(t) = K_{1,\mathrm{TX}}z(t) + K_{2,\mathrm{TX}}^{*}z^{*}(t) \qquad (3)$$

$$z_{\mathrm{RX}}(t) = K_{1,\mathrm{RX}}z(t) + K_{2,\mathrm{RX}}z^{*}(t) \qquad (4)$$

where $z(t)$ denotes the ideal baseband equivalent under perfect matching. In frequency domain, the distortion due to the

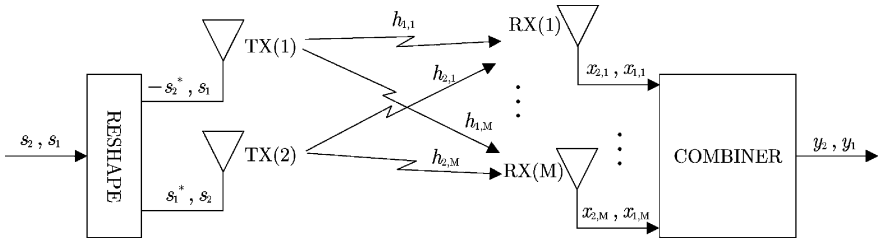

Fig. 1. Basic $2 \times M$ Alamouti diversity transmission scheme [5].

conjugate signal terms corresponds to mirror-frequency interference [17]. The corresponding mirror-frequency attenuations L_{TX} and L_{RX} of the individual front-ends are then given by

$$L_{\mathrm{TX}} = \frac{|K_{1,\mathrm{TX}}|^2}{|K_{2,\mathrm{TX}}|^2}, \quad L_{\mathrm{RX}} = \frac{|K_{1,\mathrm{RX}}|^2}{|K_{2,\mathrm{RX}}|^2} \tag{5}$$

which typically range in the order of 25–40 dB [11]–[16]. At the modeling level, to keep the overall signal power independent of the imbalance values, the TX and RX imbalance coefficients can be normalized by $1/\sqrt{|K_{1,\mathrm{TX}}|^2 + |K_{2,\mathrm{TX}}|^2}$ and $1/\sqrt{|K_{1,\mathrm{RX}}|^2 + |K_{2,\mathrm{RX}}|^2}$, respectively.

C. Space-Time Coding and MIMO System Models With I/Q Mismatch

As an example of effective space-time coded multiantenna system, we consider the so-called $2 \times M$ (two transmit antennas and M receive antennas) Alamouti diversity transmission scheme [5], [6]. The basic system setup is illustrated in Fig. 1. Given two consecutive data symbols s_1 and s_2 entering the transmitter, the idea in short is to transmit these symbols in parallel during the first signaling interval over the two transmit antennas. Then during the second signaling interval, symbols $-s_2^*$ and s_1^* are transmitted correspondingly. Denoting the baseband equivalent complex channel coefficient from the transmitter j to the receiver i by $h_{j,i}, j \in \{1,2\}, i \in \{1,2,\ldots,M\}$ (frequency-flat channels assumed here [5]), the signal samples in the ith receiver are given by

$$\begin{aligned} x_{1,i} &= h_{1,i}s_1 + h_{2,i}s_2 \\ x_{2,i} &= -h_{1,i}s_2^* + h_{2,i}s_1^*. \end{aligned} \tag{6}$$

Here, for a moment, additive noise is ignored for notational simplicity, and ideal synchronization is also assumed. Then diversity gain over the individual transmitter–receiver links can be obtained by combining the samples as

$$\begin{aligned} y_1 &= \sum_{i=1}^{M} (h_{1,i}^* x_{1,i} + h_{2,i} x_{2,i}^*) = \sum_{i=1}^{M} (|h_{1,i}|^2 + |h_{2,i}|^2) s_1 \\ y_2 &= \sum_{i=1}^{M} (h_{2,i}^* x_{1,i} - h_{1,i} x_{2,i}^*) = \sum_{i=1}^{M} (|h_{1,i}|^2 + |h_{2,i}|^2) s_2. \end{aligned} \tag{7}$$

Assuming independent channels $h_{j,i}$, it is highly unlikely that all the channels are in a bad state simultaneously and the quality of the overall link is thus improved. For more details, refer to [5].

In the above discussions, ideal radio front-end implementations are basically assumed. Now, in order to explore the I/Q mismatch effects on the overall link quality, we apply the I/Q mismatch models of (3) and (4). For generality, the $2 \times M$ case is assumed. On the transmitters side, the TX symbols are effectively distorted according to (3). These distorted TX signals travel then through the channels, and the signals arriving in the receivers are further shaped according to (4) in the individual RX front-ends. Including then also the diversity combining stage, the overall signal model for the combiner output signals under I/Q imbalance can finally be shown to be

$$\begin{aligned} y_1 &= as_1 + bs_1^* + cs_2 + ds_2^* \\ y_2 &= a^* s_2 + b^* s_2^* - c^* s_1 - d^* s_1^* \end{aligned} \tag{8}$$

where the coefficients a, b, c, and d are given in (9) at the bottom of the page. Under perfect I/Q matching in all the transmitters and receivers ($K_{1,\mathrm{TX/RX}} = 1$ and $K_{2,\mathrm{TX/RX}} = 0$),

$$\begin{aligned} a &= \sum_{i=1}^{M} \left(|h_{1,i}|^2 K_{1,\mathrm{RX}(i)} K_{1,\mathrm{TX}(1)} + |h_{2,i}|^2 K_{1,\mathrm{RX}(i)}^* K_{1,\mathrm{TX}(2)}^* + (h_{1,i}^*)^2 K_{2,\mathrm{RX}(i)} K_{2,\mathrm{TX}(1)} + (h_{2,i})^2 K_{2,\mathrm{RX}(i)}^* K_{2,\mathrm{TX}(2)}^* \right) \\ b &= \sum_{i=1}^{M} \left(|h_{1,i}|^2 K_{1,\mathrm{RX}(i)} K_{2,\mathrm{TX}(1)}^* + |h_{2,i}|^2 K_{1,\mathrm{RX}(i)}^* K_{2,\mathrm{TX}(2)} + (h_{1,i}^*)^2 K_{2,\mathrm{RX}(i)} K_{1,\mathrm{TX}(1)}^* + (h_{2,i})^2 K_{2,\mathrm{RX}(i)}^* K_{1,\mathrm{TX}(2)} \right) \\ c &= \sum_{i=1}^{M} \left(h_{1,i}^* h_{2,i} K_{1,\mathrm{RX}(i)} K_{1,\mathrm{TX}(2)} + h_{1,i}^* h_{2,i}^* K_{2,\mathrm{RX}(i)} K_{2,\mathrm{TX}(2)} - h_{1,i}^* h_{2,i} K_{1,\mathrm{RX}(i)}^* K_{1,\mathrm{TX}(1)}^* - h_{1,i} h_{2,i} K_{2,\mathrm{RX}(i)}^* K_{2,\mathrm{TX}(1)}^* \right) \\ d &= \sum_{i=1}^{M} \left(h_{1,i}^* h_{2,i} K_{1,\mathrm{RX}(i)} K_{2,\mathrm{TX}(2)}^* + h_{1,i}^* h_{2,i}^* K_{2,\mathrm{RX}(i)} K_{1,\mathrm{TX}(2)}^* - h_{1,i}^* h_{2,i} K_{1,\mathrm{RX}(i)} K_{2,\mathrm{TX}(1)} - h_{1,i} h_{2,i} K_{2,\mathrm{RX}(i)}^* K_{1,\mathrm{TX}(1)}^* \right). \end{aligned} \tag{9}$$

the model in (8) and (9) obviously reduces to the basic signal model in (7). Now, based on (8), the I/Q imbalance effect is fundamentally different compared to ordinary single-antenna systems. Here the signal is interfered not only by its own complex-conjugate [as in (3) and (4)] but also by the other information bearing signal (or signals in general) in the air during any specific signaling interval. Thus, in general, radio front-end related impairments, such as I/Q imbalance considered here, are expected to play even bigger role in multiantenna systems than in ordinary single-antenna setups. This will also be shown analytically in Section IV where the effective signal-to-distortion or signal-to-interference ratio (SIR) due to I/Q imbalance is analyzed in closed form. Notice that the signal models in (8) and (9) can be interpreted as generalizations of the simple 2×1 system considered in [23]. Notice also that philosophically, from the overall system point of view, the distortion due to I/Q imbalance resembles to some extent ordinary intersymbol interference (ISI) phenomenon but cannot be really mitigated using ordinary equalization techniques due to i) the extremely short block-length of only two data symbols and ii) the additional conjugate nature of the model evident in (8). Thus, more sophisticated signal processing techniques are needed to tackle the effect. Some novel solutions are proposed next in Section III.

In general, the focus in this paper is mainly on the I/Q imbalance related topics. Other important practical aspects in the direct-conversion radio architecture are related to the so-called dc-offset problem as well as to nonlinear signal distortion due to mixing and amplification stages [8]–[10], [12]–[16]. These issues are, however, out of the scope of this paper and are thus not considered in the continuation.

III. I/Q Imbalance Compensation Techniques

A rather obvious solution to address the I/Q mismatch problem is to consider the matching of each individual front-end separately, e.g., by using any of the earlier proposed compensation techniques targeted for single-antenna systems. However, even with two transmit and two receive antennas, there are already four radio front-ends, thus basically calling for four compensators if treated separately. Thus, more interesting and also computationally more appealing approach is then to consider the combiner output signals given in (8), and use efficiently the rich algebraic structure of the underlying signal model to mitigate the effects of all the front-ends jointly. Both training signal-based as well as blind compensation techniques using this approach are presented next. In general, the purpose of the compensation stage in our formulation is to estimate the data symbols s_1 and s_2 given the observed data y_1 and y_2 in (8) and (9).

A. Training or Pilot Signal-Based Method

Most of the practical communications systems include certain known data structures in their transmission frames, called training or pilot signals. These are typically used for channel estimation and synchronization purposes. Here, in this subsection, we also assume that such a pilot or training period is available. More specifically, for imbalance compensation purposes, we assume that there exists at least two known STC blocks (called slots hereafter), over which we set the transmit data according to

$$s_1 = s_p,\ s_2 = s_p^*,\ s_3 = s_p,\ s_4 = s_p. \tag{10}$$

Here, s_p refers to the known pilot symbol which is one of the design "parameters" in the continuation. Denoting the resulting four observations by $y_{1,p}$, $y_{2,p}$, $y_{3,p}$, and $y_{4,p}$, this yields a well-behaved 4×4 set of linear equations of the form $\mathbf{y}_p$=$\mathbf{S}_p\boldsymbol{\theta}$ where $\mathbf{y}_p = [y_{1,p},\ y_{2,p}^*,\ y_{3,p},\ y_{4,p}^*]^T$, $\boldsymbol{\theta} = [a\ b\ c\ d]^T$, and

$$\mathbf{S}_p = \begin{bmatrix} s_p & s_p^* & s_p^* & s_p \\ s_p & s_p^* & -s_p^* & -s_p \\ s_p & s_p^* & s_p & s_p^* \\ s_p^* & s_p & -s_p^* & -s_p \end{bmatrix}. \tag{11}$$

This follows directly from (8) and (10). Thus, clearly, since $\det(\mathbf{S}_p) = 2(s_p^2 - (s_p^*)^2)^2$, the "system" matrix $\mathbf{S}_p$ in (11) is non-singular and the unknown coefficient vector $\boldsymbol{\theta} = [a\ b\ c\ d]^T$ can be solved uniquely as $\hat{\boldsymbol{\theta}}$=$\mathbf{S}_p{}^{-1}\mathbf{y}_p$, given that $s_p^2 \neq (s_p^*)^2$. This, in turn, is trivially true given that the training symbol s_p is not purely real nor purely imaginary. After estimating the model coefficients $\boldsymbol{\theta} = [a\ b\ c\ d]^T$, the actual payload (information-bearing) data can then be estimated easily based on (8). Within one STC block with data symbols s_1 and s_2, according to the model in (8), the compensator outputs can formally be solved from $\mathbf{y} = \mathbf{H}\mathbf{s}_c$ where $\mathbf{y} = [y_1,\ y_1^*,\ y_2,\ y_2^*]^T$, $\mathbf{s}_c = [s_1,\ s_1^*,\ s_2,\ s_2^*]^T$, and

$$\mathbf{H} = \begin{bmatrix} \hat{a} & \hat{b} & \hat{c} & \hat{d} \\ \hat{b}^* & \hat{a}^* & \hat{d}^* & \hat{c}^* \\ -\hat{c}^* & -\hat{d}^* & \hat{a}^* & \hat{b}^* \\ -\hat{d} & -\hat{c} & \hat{b} & \hat{a} \end{bmatrix}. \tag{12}$$

In (12), $\hat{a}$, $\hat{b}$, $\hat{c}$, and $\hat{d}$ refer to the estimated coefficients. Here, instead of full inversion of $\mathbf{H}$ ($\hat{\mathbf{s}}_c = \mathbf{H}^{-1}\mathbf{y}$), $\mathbf{y} = \mathbf{H}\mathbf{s}_c$, needs to be solved only for $[\mathbf{s}_c]_1 = s_1$ and $[\mathbf{s}_c]_3 = s_2$, which together with the obvious symmetry in (12), results in big savings in the computational complexity. The effects of additive noise together with other practical aspects will be discussed and addressed in Section III-C.

B. Blind Compensation Using Blind Signal Separation

Instead of relying on the availability of the known pilot signals, another interesting approach is to address the imbalance compensation using blind signal estimation techniques. In general, the so-called blind signal separation (BSS) task deals with recovering some interesting signals, called sources, based on observing their linear mixtures only. Typically the strong assumption of *statistical independence* of the assumed source signals is utilized, to form the basis for the actual signal estimation algorithms; see, e.g., [31]–[33] for excellent discussions and descriptions of the most common approaches.

In our context, the observed signals within one STC block obey (8), meaning that the observed data y_1 and y_2 appear as linear combinations of four formal source signals s_1, s_1^*, s_2, and s_2^*. However, this viewpoint does not lend itself very

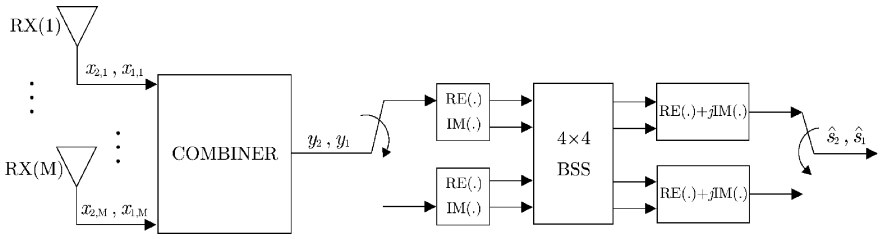

Fig. 2. Blind I/Q separation based compensation structure.

well to the general blind signal estimation since the conjugated signal pairs are obviously statistically dependent. Notice that the circularity assumption ($E[s_i^2(t)] = 0$) actually does imply that s_i and s_i^* are indeed mutually *uncorrelated*, but this second-order statistics is yet insufficient here alone for blind signal recovery. We can, however, view the observed complex signals y_1 and y_2 in (8) in terms of their I and Q components, resulting in four real-valued observations $y_{1,I} = \mathrm{Re}[y_1]$, $y_{1,Q} = \mathrm{Im}[y_1]$, $y_{2,I} = \mathrm{Re}[y_2]$ and $y_{2,Q} = \mathrm{Im}[y_2]$. Using a similar approach for the formal source signals s_1 and s_2, results in the following 4×4 real-valued signal model of the form $\mathbf{y}_{IQ} = \mathbf{H}_{IQ}\mathbf{s}_{IQ}$ where $\mathbf{y}_{IQ} = [y_{1,I},\ y_{1,Q},\ y_{2,I},\ y_{2,Q}]^T$, $\mathbf{s}_{IQ} = [s_{1,I},\ s_{1,Q},\ s_{2,I},\ s_{2,Q}]^T$, and

$$\mathbf{H}_{IQ} = \begin{bmatrix} \mathrm{Re}(a+b) & -\mathrm{Im}(a-b) & \mathrm{Re}(c+d) & -\mathrm{Im}(c-d) \\ \mathrm{Im}(a+b) & \mathrm{Re}(a-b) & \mathrm{Im}(c+d) & \mathrm{Re}(c-d) \\ -\mathrm{Re}(c+d) & \mathrm{Im}(c-d) & \mathrm{Re}(a+b) & -\mathrm{Im}(a-b) \\ -\mathrm{Im}(c+d) & -\mathrm{Re}(c-d) & \mathrm{Im}(a+b) & \mathrm{Re}(a-b) \end{bmatrix}. \tag{13}$$

This follows directly from (8). Now assuming that the I and Q components of the data symbols are all mutually independent, the source signals $\mathbf{s}_{IQ}$ can be blindly estimated based on observed data $\mathbf{y}_{IQ}$. This assumed independence of I and Q, in turn, basically holds for any of the standard QAM type symbol constellations and also up to a certain degree to PSK type constellations (see the discussions in single-input single-output context in [20] and [21]). Notice that since the model $\mathbf{y}_{IQ} = \mathbf{H}_{IQ}\mathbf{s}_{IQ}$ holds for any pair of two consecutive data symbols, either block-based or adaptive BSS algorithms can basically be applied. Here, in the performance simulations in Section V, the well-known equivariant adaptive separation via independence (EASI) algorithm [33] is used in implementing the separation stage. Denoting the separator coefficients at discrete-time index k by $\mathbf{B}_{IQ}(k)$, the formal output of the compensator is simply $\hat{\mathbf{s}}_{IQ}(k) = \mathbf{B}_{IQ}(k)\mathbf{y}_{IQ}(k)$. One iteration of the coefficient adaptation, in turn, is given by [33]

$$\mathbf{B}_{IQ}(k+1) = \mathbf{B}_{IQ}(k) - \mu\left[\frac{\hat{\mathbf{s}}_{IQ}(k)\hat{\mathbf{s}}_{IQ}(k)^T - \mathbf{I}}{1+\mu\hat{\mathbf{s}}_{IQ}(k)^T\hat{\mathbf{s}}_{IQ}(k)} + \frac{\mathbf{g}(\hat{\mathbf{s}}_{IQ}(k))\hat{\mathbf{s}}_{IQ}(k)^T - \hat{\mathbf{s}}_{IQ}(k)\mathbf{g}(\hat{\mathbf{s}}_{IQ}(k))^T}{1+\mu\left|\hat{\mathbf{s}}_{IQ}(k)^T\mathbf{g}(\hat{\mathbf{s}}_{IQ}(k))\right|}\right]\mathbf{B}_{IQ}(k) \tag{14}$$

where μ is the adaptation step-size and $\mathbf{g}(\cdot)$ is a memoryless nonlinear function which is typically selected based on the assumed source statistics. For more details on the algorithm and signal separation in general, refer to [33]. In this context, it is also interesting to note that at purely BSS algorithm development level, there's been some work recently [34] addressing the general task of separation of complex sources using the I/Q decomposition idea. Notice, however, that the philosophical viewpoints here and in [34] are basically different—splitting the two complex signals and the resulting observations is here *needed* in order to have a uniquely identifiable model for the separation, independently of the applied BSS algorithm, while in [34] the assumed independence of the I and Q of the underlying complex signals is built-in to the separation algorithm itself. Here, using the model in (13), *any BSS algorithm* can basically be applied. The overall compensation idea is further illustrated graphically in Fig. 2 at a conceptual level.

In general, the blind signal separation task has two indeterminacies – the order and scaling of the output signals [31]–[33]. Here, however, the structure of the effective mixing matrix in (13) is such that the diagonal elements are an order of magnitude larger (in absolute values) compared to the off-diagonal elements, and thus in practice, the separator always converges towards the correct ordering of the source signals. Using (14), see also [33], the variance of the output components, in turn, is essentially fixed to unity, and thus proper scaling of the estimated I and Q components can be restored simply based on the known variance of the used data constellation. Thus, it can be concluded that the typical permutation and scaling problems related to BSS in general are here avoided, which is seen very important for practical applications.

C. Practical Aspects and Architectural Issues

One important practical aspect in any communication system is the presence of additive noise. Here, in the pilot based compensation concept, the critical part is the coefficient estimation accuracy, which is obviously affected by noise. However, using simple averaging over a few consecutive training slots yields compensation performance virtually identical to the perfectly matched case. Illustrations will be given in Section V. The noise obviously has some influence also on the BSS based compensator, but since the whole idea is based on directly estimating the data signals instead of any parameters of a parametric model, the resulting performance is not expected to be seriously degraded at reasonable noise levels. This will also be shown to hold through simulations in Section V.

Another crucial aspect here is the role of the channel coefficients. The basic starting point in the whole transmission concept is the assumption that the channel is time-invariant

at least over two consecutive signaling intervals. In the compensation context, since the model coefficients in (9) depend on the channel properties, a time-invariant channel needs to be assumed over a longer block of data. In the pilot based compensation scheme, this is needed to keep the pilot overhead reasonable such that the estimated model coefficients can be used to process the actual payload data. Notice that this assumption needs to be made anyway in practice from the channel estimation and tracking point of view. In the BSS based compensation scheme, on the other hand, a time-variant channel simply means that the mixture coefficients in (13) are time-varying as well. In principle, with slowly fading channels, this can be tracked with adaptive BSS techniques, such as the one described in [33]. However, in order to reach the perfectly matched system performance, time-invariant channel needs to be assumed also in this context, over a reasonable processing block length. Thus, a very rapidly fading channel can be seen as one practical limitation of the proposed techniques. In general, these types of "block-fading" assumptions are, however, rather typical in most system and algorithm level developments in the literature.

In practice, with or without imbalance, the accuracy of the *channel estimates* is also critical from the system performance point of view. In general, both I/Q imbalance and additive noise complicate the channel estimation task, resulting in errors in the estimated channel coefficients. The use of incorrect channel coefficients in the diversity combining, in turn, results in a formally identical signal model as in (8) but with modified values for the system coefficients a, b, c, and d. However, since both compensators are essentially estimating these coefficients, either explicitly or implicitly, the compensated system performance is not affected by the errors in channel estimation. Thus, by design, both proposed compensation techniques are not only robust against channel estimation errors but actually also compensate for their effects together with the I/Q impairments. This is one clear practical benefit, and will be further demonstrated using simulations in Section V.

One additional practical problem in any communication system is related to the *carrier synchronization*. In our context, this is especially important since the compensator is operating on the combined front-end signals. More specifically, under carrier frequency offset (CFO) $\Delta\omega = 2\pi\Delta f$, the basic receiver model in (4) is first effectively modified such that $K_{1,\mathrm{RX}} \leftarrow K_{1,\mathrm{RX}}\exp(j\Delta\omega t)$ and $K_{2,\mathrm{RX}} \leftarrow K_{2,\mathrm{RX}}\exp(-j\Delta\omega t)$ (see, e.g., the discussions in [21] in the single-antenna system context). Assuming now that the frequency offset $\Delta\omega$ can be estimated in the RX digital front-end(s), de-rotation of the RX front-end signals, prior to the diversity combining stage, yields then essentially $K_{1,\mathrm{RX}}\exp(j\Delta\omega t)\times\exp(-j\Delta\omega t) = K_{1,\mathrm{RX}}$ and $K_{2,\mathrm{RX}}\exp(-j\Delta\omega t)\times\exp(-j\Delta\omega t) = K_{2,\mathrm{RX}}\exp(-j2\Delta\omega t)$. Thus, overall this means that $K_{2,\mathrm{RX}(i)} \leftarrow K_{2,\mathrm{RX}(i)}\exp(-j2\Delta\omega t)$ which implies that the effective system coefficients a, b, c, and d become time-varying (oscillating). This, of course, complicates then also the compensation. Thus, in this sense, it is fair to say that using separate I/Q imbalance compensators operating individually on each of the transmitters and receivers front-ends would offer more robustness against carrier frequency offsets, compared to the joint compensation approach utilized here. It should be noted, however, that with practical imbalance levels, the *range* of the system coefficients a, b, c, and d within which the time-variations due to CFO occur is fairly limited, and thus with some averaging in the compensator parameter estimation stage, reliable compensation is still obtained. This applies to both the training based as well as the blind compensator, and will be demonstrated in Section V.

IV. Signal-to-interference Ratio Analysis and Numerical Illustrations

In the following, we analyze the average total signal-to-interference ratio (SIR) at the combiner output due to I/Q imbalance using the signal models of the previous sections. In general, based on (8), the total interference consists of the self-interference term (relative to the conjugate of the target symbol) as well as of the effect of the other symbol transmitted simultaneously. The natural interference-free reference signals with perfect I/Q balance are $\sum_{i=1}^{M}(|h_{1,i}|^2+|h_{2,i}|^2)s_1$ and $\sum_{i=1}^{M}(|h_{1,i}|^2+|h_{2,i}|^2)s_2$ as given in (7). To simplify some of the forthcoming expressions and definitions, the notation $h_{\mathrm{tot}} = \sum_{i=1}^{M}(|h_{1,i}|^2+|h_{2,i}|^2)$ is used in the following.

In the analysis, we assume that the channel coefficients $h_{1,i}$ and $h_{2,i}$ are statistically independent complex circular (see [30] for excellent treatment of circular/noncircular random signals and their essential second-order statistics) Gaussian random variables with zero mean and equal mean power $E[|h_{1,i}|^2] = E[|h_{2,i}|^2] = P_h$. From this it basically follows that i) $E[h_{1,i}^2] = E[h_{2,i}^2] = 0$, ii) $E[|h_{1,i}|^2 h_{1,i}^2] = E[|h_{2,i}|^2 h_{2,i}^2] = 0$, and iii) $E[|h_{1,i}|^4] = 2(E[|h_{1,i}|^2])^2 = 2(E[|h_{2,i}|^2])^2 = E[|h_{2,i}|^4] = 2P_h^2$ which simplify the analysis and notations. We further assume that also the data symbols s_1 and s_2 are equal-variance, mutually uncorrelated ($E[s_1 s_2^*] = 0 = E[s_1^* s_2]$) and circular ($E[s_1^2] = 0 = E[s_2^2]$), as well as jointly circular ($E[s_1 s_2] = 0$). These assumptions can in general be seen rather feasible from the practical data structures (modulation, etc.) point of view.

Now, consider first the combiner output y_1. Based on (7) and (8), and the previous assumptions on the second-order statistics of the data symbols s_1 and s_2, the SIR can be defined as

$$\mathrm{SIR} = \frac{E\left[|h_{\mathrm{tot}}|^2\right]}{E\left[|(a-h_{\mathrm{tot}})|^2\right] + E\left[|b|^2\right] + E\left[|c|^2\right] + E\left[|d|^2\right]}. \tag{15}$$

In (15), it is also assumed that the data symbols s_1 and s_2 are independent of the channel coefficients $h_{1,i}$, and $h_{2,i}$, which is of course physically plausible. Based on (7) and (8), and the earlier assumptions on s_1, s_2 and $h_{1,i}$, $h_{2,i}$, this is also the SIR for the second combiner output y_2. Now using the expressions in (9) for the system coefficients a, b, c, and d, combined with the previous assumptions on the channel and data statistics, the SIR in (15) can finally be written as

$$\mathrm{SIR} = \frac{4M^2+2M}{\rho(M)} \tag{16}$$

TABLE I
EXAMPLE OF THE INFLUENCE OF PHASE IMBALANCE SIGN ON THE TOTAL AVERAGE SIR DUE TO I/Q IMBALANCE IN A 2×2 STTD SYSTEM

	Imbalance Values				SIR [dB]
	TX1	TX2	RX1	RX2	
Case 1	4%, 4°	3%, 3°	5%, 5°	5%, 5°	26.0
Case 2	4%, 4°	3%, 3°	5%, 5°	5%, −5°	23.8
Case 3	4%, −4°	3%, −3°	5%, 5°	5%, 5°	22.4

in which $\rho(M)$ is given by (17), shown at the bottom of the page. Notice that the SIR in (16) and (17) is fully determined by the imbalance coefficients and the number of receivers, and can be directly evaluated for any possible imbalance scenario and/or number of receivers without any data or system simulations. As a simple numerical example (for $M = 1$), with 5% and -5 degrees receiver imbalances and transmitter imbalances of 4% and 4 degrees (TX1) and 3% and 3 degrees (TX2), the average SIR at the combiner output is 20.2 dB, as can be evaluated using (16) and (17). Especially with higher order spectrally efficient modulation methods, such as 16PSK or 64QAM, this results in a severe reduction in the system noise margin, and thus some additional signal processing (analog or digital) is generally needed. Notice that based on (5), the individual analog front-end image attenuations are roughly 26.0 dB (RX), 27.9 dB (TX1), and 30.4 dB (TX2). Thus, the SIR figure of 20.2 dB is really *considerably lower* than what might have been expected by considering the qualities of the individual analog front-ends alone. This is due to the cross-coupling interference evident in (8), with the total obtainable SIR performance being analytically characterized by (16) and (17). This is one of the core contributions of this paper in general. It should also be noted, however, that the *distribution of the interference* is *not* exactly Gaussian (even with Gaussian channel coefficients), and also that the self-interference part of the total interference is obviously statistically dependent on the desired signal term. Thus, the derived SIR cannot necessarily be directly mapped (one-to-one) to the lowest achievable detection error probability. Instead, computer simulations are used in Section V to assess the *exact* error rate performance. Based on those results, the derived SIR in (16)–(17) does anyway give clear indication on the relative system or detection performance with, e.g., different imbalance levels, without having to resort to lengthy data and system simulations.

Closer examination of the previous results in (16) and (17) indicate some further interesting aspects in assessing the role of I/Q imbalance in multiantenna systems. One interesting issue is the role of *relative signs* between the phase imbalance values $\phi_{\mathrm{TX}(1)}$, $\phi_{\mathrm{TX}(2)}$ and $\phi_{\mathrm{RX}(i)}$, $i = 1,2,\ldots,M$. More specifically, based on (17), the resulting SIR does not depend only on the absolute values of the imbalances. As a concrete example with $M = 2$, some resulting numerical SIR values are shown in Table I, obtained here with fixed absolute imbalance levels and by just changing the relative signs of $\phi_{\mathrm{TX}(1)}$, $\phi_{\mathrm{TX}(2)}$, $\phi_{\mathrm{RX}(1)}$ and $\phi_{\mathrm{RX}(2)}$. Here best SIR is obtained when all the signs are the same while the worst case happens when $\phi_{\mathrm{TX}(1)}\phi_{\mathrm{TX}(2)}\phi_{\mathrm{RX}(1)}\phi_{\mathrm{RX}(2)} < 0$, $\phi_{\mathrm{TX}(1)}\phi_{\mathrm{TX}(2)} > 0$, and $\phi_{\mathrm{RX}(1)}\phi_{\mathrm{RX}(2)} > 0$. Notice that it is indeed the relative strength of the cross-coupling interference stemming from the other transmitted symbol which depends heavily on the phase imbalance signs, being thus specific issue to multiantenna transmission schemes. To get some visual justification for the reported SIR figures, the corresponding example symbol constellations are shown in Fig. 3. Here the data is 16QAM modulated, random Gaussian channel coefficients are used, and for clarity there is no additive channel noise, meaning that ideal 16QAM constellations would be obtained under perfect I/Q balance. Clearly the difference in the derived SIR values is

$$
\begin{aligned}
\rho(M) = {} & 3\sum_{i=1}^{M}\left(\left|K_{1,\mathrm{RX}(i)}K_{1,\mathrm{TX}(1)}\right|^2 + \left|K^*_{1,\mathrm{RX}(i)}K^*_{1,\mathrm{TX}(2)}\right|^2 + \left|K_{2,\mathrm{RX}(i)}K_{2,\mathrm{TX}(1)}\right|^2 + \left|K^*_{2,\mathrm{RX}(i)}K^*_{2,\mathrm{TX}(2)}\right|^2\right) \\
& + 3\sum_{i=1}^{M}\left(\left|K_{1,\mathrm{RX}(i)}K^*_{2,\mathrm{TX}(1)}\right|^2 + \left|K^*_{1,\mathrm{RX}(i)}K_{2,TX(2)}\right|^2 + \left|K_{2,\mathrm{RX}(i)}K^*_{1,\mathrm{TX}(1)}\right|^2 + \left|K^*_{2,\mathrm{RX}(i)}K_{1,\mathrm{TX}(2)}\right|^2\right) \\
& + 2\sum_{i=1}^{M-1}\sum_{j=i+1}^{M}\mathrm{Re}[(\left|K_{1,\mathrm{TX}(1)}\right|^2 + \left|K_{1,\mathrm{TX}(2)}\right|^2 + \left|K_{2,\mathrm{TX}(1)}\right|^2 + \left|K_{2,\mathrm{TX}(2)}\right|^2)K_{1,\mathrm{RX}(i)}K^*_{1,\mathrm{RX}(j)}] \\
& + 2\sum_{i=1}^{M}\sum_{\substack{j=1\\ j\neq i}}^{M}\mathrm{Re}[K^*_{1,\mathrm{RX}(i)}K^*_{1,\mathrm{TX}(2)}K^*_{1,\mathrm{RX}(j)}K^*_{1,\mathrm{TX}(1)} + K_{1,\mathrm{RX}(i)}K^*_{2,\mathrm{TX}(1)}K_{1,\mathrm{RX}(j)}K^*_{2,\mathrm{TX}(2)}] \\
& - (4M+2)\sum_{i=1}^{M}\mathrm{Re}[K_{1,\mathrm{RX}(i)}K_{1,TX(1)} + K^*_{1,\mathrm{RX}(i)}K^*_{1,\mathrm{TX}(2)}] + (4M^2+2M). \qquad (17)
\end{aligned}
$$

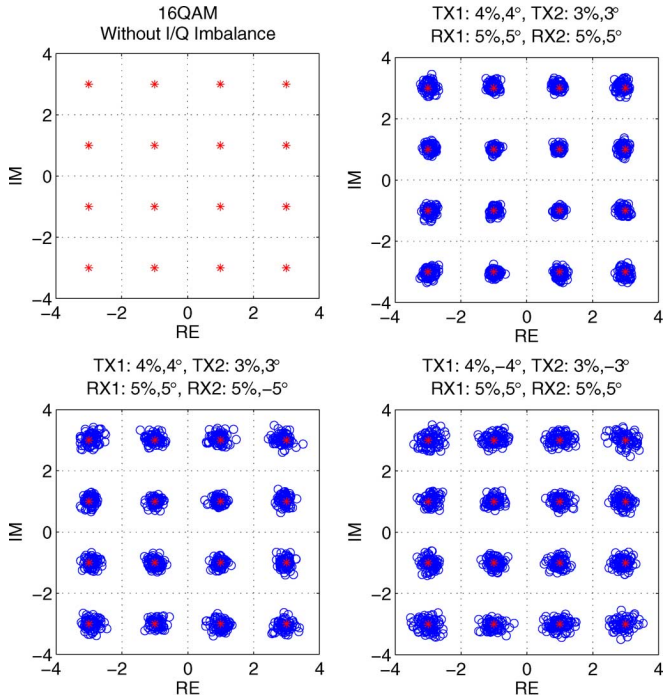

Fig. 3. 16QAM symbol rate constellations with different phase imbalance signs in a 2×2 STTD system. Gaussian channels and no additive noise. The corresponding SIR values are reported in Table I.

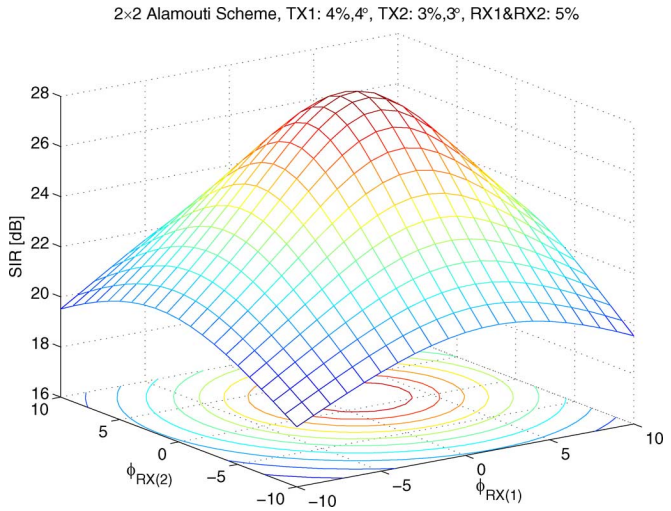

Fig. 4. SIR as a function of the receiver phase imbalances in a 2×2 STTD system.

visible also in the quality of the corresponding constellations. Notice that the image attenuations of the individual front-ends (TX1,2 and RX1,2) are identical in all the three cases. This shows that traditional imbalance analysis using the image attenuations of the individual front-ends alone is insufficient.

To further illustrate the complex nature of the mapping between the individual RX and TX imbalances and the overall achievable SIR, the previous case of 4%, 4 degrees (TX1) and 3%, 3 degrees (TX2) transmitter imbalances is considered and the two receivers' *amplitude imbalances* are both set to 5%. Then the achievable SIR is evaluated with varying the *phase imbalances* for the two receivers. The results are shown in Fig. 4.

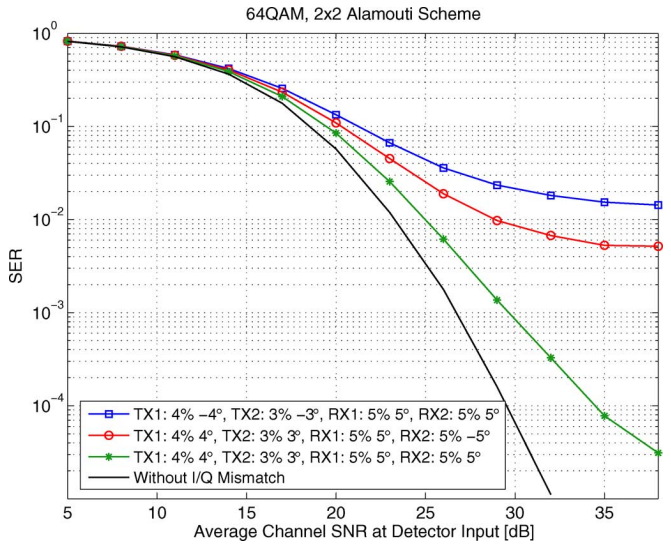

Fig. 5. Detection error rate for 2×2 64QAM STTD system with three different imbalance values (different phase imbalance signs). Also shown for reference is the corresponding perfectly matched system performance.

Notice that the point of maximum SIR does not exactly match the case of perfect phase matching for the two receivers.

V. Performance Simulations

Comprehensive computer simulations are carried out next to assess the performance of the Alamouti space-time transmit diversity system under I/Q imbalance, and especially to demonstrate the good compensation performance of the proposed compensation techniques. More specifically, the 2×2 system scenario is assumed, and 64QAM is used as the modulation method, representing a spectrally efficient data constellation being likely to be deployed in future wireless systems. The actual performance measure is here symbol error rate (SER) in the data detection stage. All the comparisons are made against a perfectly matched reference system with perfect I/Q balance. Also the connections to the previous SIR analysis are addressed. In all the simulations, a minimum of 1 000 000 data symbols are used in evaluating the detection error rates. Naturally the system model also includes additive white Gaussian noise, and as earlier in the analysis, the channel coefficients are drawn randomly from complex Gaussian distribution. The effects of channel estimation errors and residual frequency offsets are also examined.

A. I/Q Imbalance and Detection Error Rates

Fig. 5 presents the obtained SER as a function of average received signal-to-noise ratio (SNR) at the detector input. Three cases with different phase imbalance signs are demonstrated, resulting in considerably different error rate performance as can be seen in the figure. This was already predicted by the SIR analysis in the previous Section, without any data simulations, with the corresponding SIR values being reported in Table I. As discussed earlier, the SIR values cannot be directly paralleled to the additive noise SNR since the distribution of the interference is not exactly Gaussian. They do, however, give clear indication of the relative system performance with different imbalance

values, and thus form a useful quality measure in the analysis and design of practical systems. The SIR values also do indeed predict, in cases 1 and 2 with good accuracy, the error rate floors when compared against the perfectly matched reference system performance at the corresponding additive white Gaussian noise SNR. In general with 64QAM data, when evaluated at the raw (uncoded) SER levels of 10^{-1} and 10^{-2}, which are of practical interest in most systems before error-control decoding, the degradation due to I/Q imbalance is roughly 1 to 2.5 dB at 10^{-1} and already 2 dB to almost 15 dB at 10^{-2}. It is obvious that this kind of performance losses are unacceptable in any practical system, and thus signal enhancement through efficient compensation processing is definitely needed. Notice again that the image attenuations of the individual analog front-ends are identical in all the three cases.

B. Obtained Compensation Performance

Here the detection error rate performance of the compensated system is demonstrated, using both the training based as well as blind compensation methods proposed earlier in Section III. The "intermediate" case of the previously demonstrated imbalance values (4% and 4 degrees (TX1), 3% and 3 degrees (TX2), 5% and 5 degrees (RX1), 5% and -5 degrees (RX2)) is used to model a typical example case. In general, virtually all the signal distortion due to I/Q imbalance can be efficiently removed using either of the proposed techniques, the error rate performance being within 0.2 dB of the perfectly matched reference, as will be demonstrated in the following subsections. This is one of the main reasons why no further comparison against possible other compensation techniques (other than the perfectly matched reference system) is needed. Also the computational complexity of both techniques is more than feasible for already today's state-of-the-art digital signal processing implementations. Detailed analysis of the exact computational complexity in terms of complex multiplications and additions is, however, left for future studies.

1) Pilot Based Compensator: As explained earlier in Section III.A, the idea is to estimate the "system" coefficients a, b, c, and d using known pilot data, and then use these estimates during the actual data transmission phase to estimate the data symbols s_1 and s_2 from (8). Here different numbers of pilot slots are tested and the upper-right corner symbol ("$7+7j$") from the 64QAM constellation is selected as the used pilot symbol. Using the symbol with biggest amplitude as the pilot data is rather standard technique in most practical systems (corresponding to roughly 3.5 dB pilot "boosting" compared to average constellation power). The channel coefficients are again drawn randomly from complex Gaussian distribution. Furthermore, a quasi-static system model is also assumed in the sense that the channels are assumed fixed over 1000 consecutive signaling intervals, after which new channel coefficients are drawn independently. The known pilot data appears in the beginning of each 1000 symbol block, and altogether 1 000 000 data symbols are used in evaluating the error rates.

The obtained performance with varying number of pilot slots is depicted in Fig. 6, together with the uncompensated as well as perfectly matched reference cases. Clearly, due to the additive channel noise, estimation accuracy based on one pilot slot alone is insufficient. However, averaging over five pilots yields already performance really close to that of the reference system, the difference being here roughly 0.2 dB. Thus, it can be concluded that all the essential signal distortion due to I/Q imbalance can be efficiently compensated using the proposed technique. In general, depending on the amount of used pilot overhead, the gain due to compensation processing is from around 3 dB close to 7 dB, when measured at uncoded (raw) SER level of 10^{-2}. Conceptually, it is also very important to note that the diversity gain obtained from the overall transmission scheme is *not* affected by the compensation processing. This can be established from the shown performance results by noting that the *slopes* of the compensated system error rate curves are identical to that of the perfectly matched one at high SNR region.

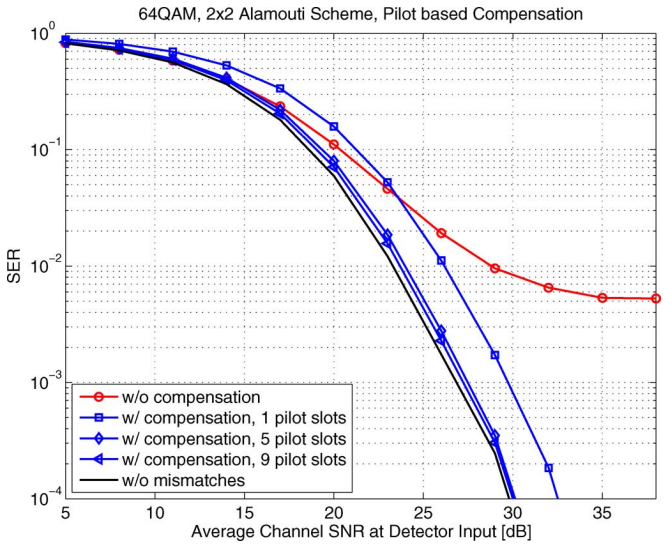

Fig. 6. Average symbol error rate (SER) performance using the proposed pilot based I/Q imbalance compensation scheme. The corresponding uncompensated and perfectly matched SER characteristics are also shown for reference. Imbalance values: 4% and 4 degrees (TX1), 3% and 3 degrees (TX2), 5% and 5 degrees (RX1), 5% and -5 degrees (RX2).

2) Blind Compensation Using I/Q BSS: An alternative compensation structure based on blind signal separation principles was also proposed in Section III, operating on the I/Q decomposition of the received complex signal blocks. Here we use the well-known EASI algorithm proposed originally in [33], and recapitulated in (14), for the actual separation implementation. A standard third-order (cubic) nonlinearity is used and the separator is always initialized with an identity matrix. Notice that this represents just one possible algorithm selection and basically any other BSS algorithm could be applied as well in practice. After drawing again the complex channel coefficients randomly from the complex Gaussian distribution, a block of 10 000 data symbols is transmitted and the received data is processed using the BSS based compensator as explained in Section III-B. So blocks of two consecutive complex samples are "split" into their I and Q components and fed into a 4×4 signal separator implemented here using the EASI algorithm. The adaptation step-size of the algorithm is selected such that convergence is established in 3000–4000 iterations. After convergence, the whole block of data is processed using the converged coefficients. This procedure is then repeated for

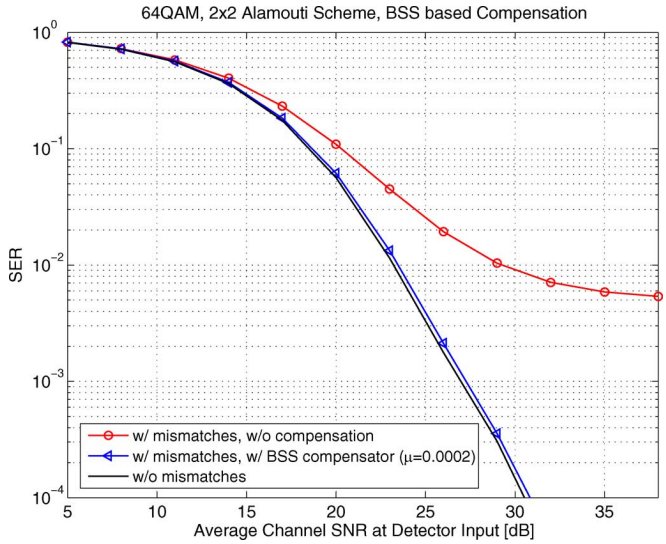

Fig. 7. Average symbol error rate (SER) performance using the proposed blind signal separation based I/Q imbalance compensation scheme. The corresponding uncompensated and perfectly matched SER characteristics are also shown for reference. Imbalance values: 4% and 4 degrees (TX1), 3% and 3 degrees (TX2), 5% and 5 degrees (RX1), 5% and −5 degrees (RX2).

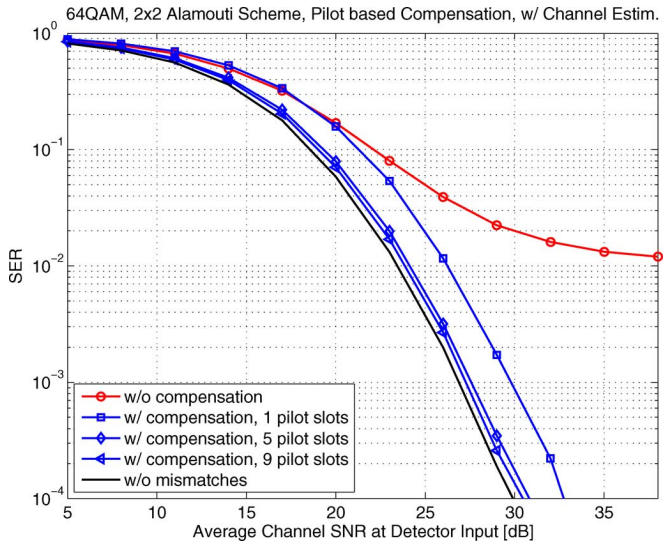

Fig. 8. Average symbol error rate (SER) performance of the pilot based imbalance compensator with channel estimation errors included. Perfectly matched reference is also shown assuming no I/Q imbalances and perfect channel estimation.

1000 independent channel realizations to assess the average performance with respect to the channel statistics.

The obtained average symbol error rate performance as a function of additive noise level is illustrated in Fig. 7. Clearly, the proposed BSS based compensation scheme can virtually remove all the signal distortion due to I/Q imbalance, the error rates of the compensated and perfectly matched "reference" systems being practically identical. When measured again at uncoded (raw) SER level of 10^{-2}, the gain due to compensation processing is here almost 7 dB. Furthermore, similarly to the pilot based compensation structure, it can be established that the signal separation stage does *not* affect the available system diversity gain, since the slopes of the compensated error rate and the perfectly matched system are again identical at high SNR.

C. Channel Estimation Errors and Frequency Offsets

Next the channel estimation task as well as receiver frequency offset are included in the signal generation model. Considering first the channel estimation, a practical channel estimator utilizing the pilot allocation given in (10) is obtained as follows. Given the first half of the pilot slot for which $s_1 = s_p, s_2 = s_p^*$, the corresponding receiver front-end samples at receiver $i \in \{1,2,\ldots,M\}$ are $x_{1,i,p} = h_{1,i}s_p + h_{2,i}s_p^*$ and $x_{2,i,p} = -h_{1,i}s_p + h_{2,i}s_p^*$, as is easy to see based on (6) and (10). Then a direct "zero-forcing" type estimator for the channel coefficients $h_{1,i}$ and $h_{2,i}$ is obtained from

$$\mathbf{x}_{i,p} = \begin{bmatrix} x_{1,i,p} \\ x_{2,i,p} \end{bmatrix} = \begin{bmatrix} s_p & s_p^* \\ -s_p & s_p^* \end{bmatrix} \begin{bmatrix} h_{1,i} \\ h_{2,i} \end{bmatrix} = \bar{\mathbf{S}}_p \mathbf{h}_i \qquad (18)$$

as $\hat{\mathbf{h}}_i = \bar{\mathbf{S}}_p^{-1}\mathbf{x}_{i,p}$. In practice, averaging over multiple pilot slots can of course be used to diminish the effects of noise and other interference. Now similar simulations as earlier are carried out in the 2×2 STTD context but utilizing the above channel estimation procedure in the two receivers. For simplicity, only a single pilot slot is utilized for channel estimation, resulting in

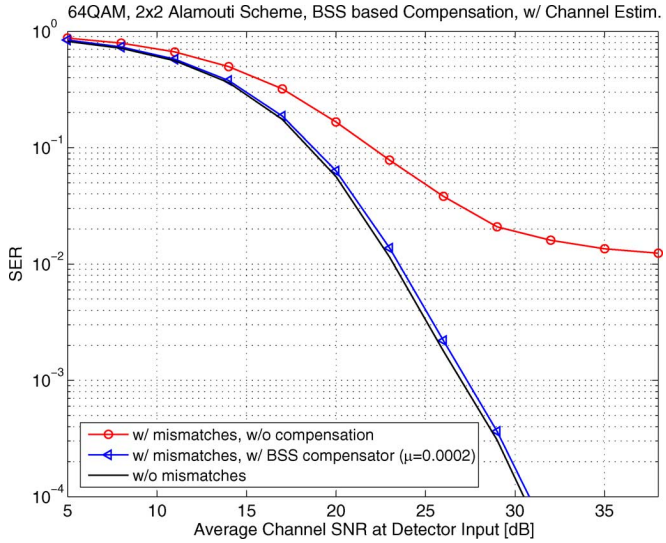

Fig. 9. Average symbol error rate (SER) performance of the blind signal separation based imbalance compensator with channel estimation errors included. Perfectly matched reference is also shown assuming no I/Q imbalances and perfect channel estimation.

rather crude channel estimates due to noise and I/Q imbalances, to be used then in diversity combining. The obtained performances of the pilot based as well as blind imbalance compensators are shown in Figs. 8 and 9, respectively. Clearly, the compensated system performances are identical to the earlier cases, which shows important robustness against channel estimation inaccuracies. Notice that the perfectly matched reference curves in Figs. 8 and 9 assume perfect I/Q balance and ideal channel estimation, so the compensators are not only mitigating the I/Q imbalance effects but also the effects of channel estimation errors (at the same time, with zero additional cost), which is an important practical asset.

Next additional system simulations are carried out with carrier frequency offset of roughly 1% of the symbol rate

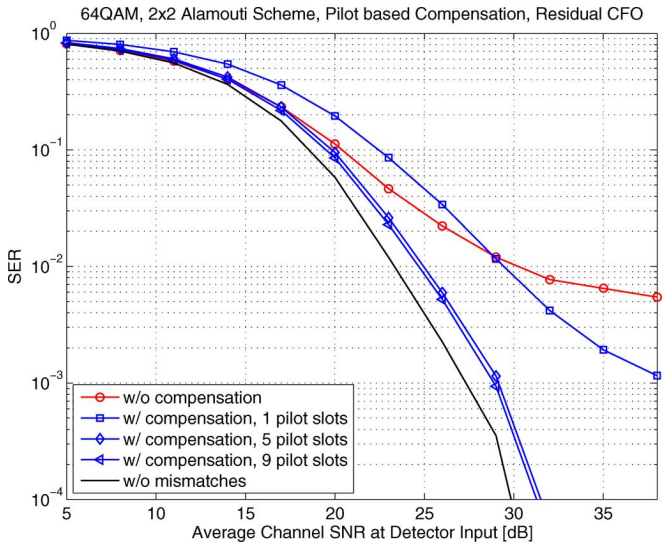

Fig. 10. Average symbol error rate (SER) performance of the pilot based imbalance compensator with $\sim 1\%$ carrier frequency offset in the receiver. Perfectly matched reference is also shown assuming no I/Q imbalances and perfect synchronization.

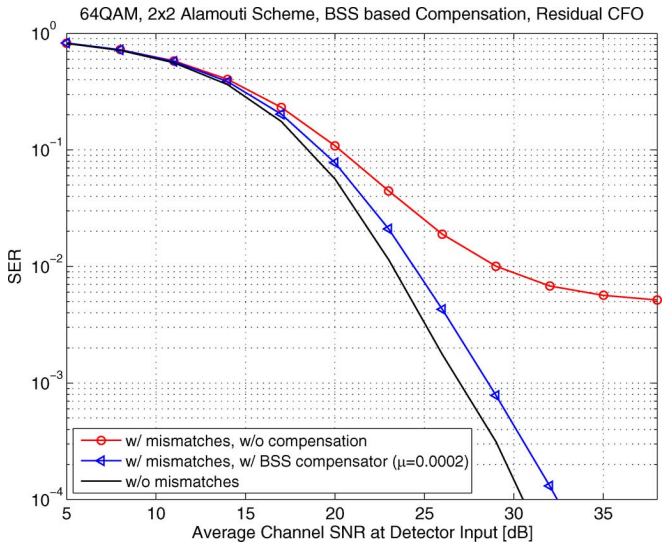

Fig. 11. Average symbol error rate (SER) performance of the blind signal separation based imbalance compensator with $\sim 1\%$ carrier frequency offset in the receiver. Perfectly matched reference is also shown assuming no I/Q imbalances and perfect synchronization.

included in the receiver front-ends. Like discussed earlier, even with proper de-rotation in the digital front-ends, this has the effect of making the effective system coefficients to vary (rotate) in time, through $K_{2,\mathrm{RX}(i)} \leftarrow K_{2,\mathrm{RX}(i)} \exp(-j2\Delta\omega t)$, and thus some performance degradation is expected. The obtained results are shown in Figs. 10 and 11. In the pilot based compensator, averaging over multiple pilot slots results in compensator coefficients corresponding to the average system coefficients and similar averaging effect is also taking place implicitly in the BSS compensator since the dynamics of the EASI algorithm with the used step-size is much slower than the time-variation rate of the system coefficients. Processing the received data then with these "average" coefficients cannot, of course, yield perfect compensation but is clearly seen to work, the performance difference being within 1 dB or so when compared to the previous simulations without carrier offsets.

Finally, we shortly address the actual *CFO estimation* task in the STC system context, assuming the same pilot allocation given in (10). In principle, without additive noise and I/Q imbalance, the CFO causes an *additional* phase change of $\Delta\omega$ [rad] between each consecutive sample in the individual receiver front-ends, prior to the diversity combining. Then, assuming that a minimum of two *pilot slots* is deployed in the system, the phase of any of the pilot elements is changing *from one pilot slot to another* by $(4+4D)\Delta\omega$ in which D denotes the number of *data slots* (each having four data symbols) inbetween two consecutive pilot slots. Thus, a relatively simple CFO estimator is obtained directly as

$$\widehat{\Delta\omega}_{p_1,i,p_2} = \frac{1}{4+4D} \angle\{x_{p_1,i}^{(p_2+1)} \times (x_{p_1,i}^{(p_2)})^*\} \qquad (19)$$

in which $p_1 = 1,2,\ldots,4$, $i = 1,2,\ldots,M$, $p_2 = 1,2,\ldots$. Here p_1 denotes the sample index inside one pilot slot, p_2 denotes the pilot slot index, i is the receiver index, $\angle\{x\}$ denotes the phase angle of a complex variable x, and thus $x_{p_1,i}^{(p_2)}$ is the p_1th sample of p_2th pilot slot in the ith receiver. Obviously noise and I/Q imbalance affect the CFO estimator, and thus averaging over the individual estimates (within each pilot slot, between different pilot slots, and possibly also between different receivers) can be used again to increase the estimator reliability. In general, the range of identifiable CFOs using (19) is easily shown to be $\pm F_{\mathrm{sym}}/(2(4+4D))$ [Hz] in which F_{sym} denotes the system symbol rate. Then, a final set of system simulations is carried out with CFO of $\sim 1\%$ of the symbol rate, including also the CFO estimator in (19). As a practical example, it is assumed that altogether ten pilot slots are implemented, with $D = 5$ data slots appearing between the neighboring pilot slots. This yields an estimation range of $\pm F_{\mathrm{sym}}/48$ or roughly 2% of the symbol rate. All ten pilot slots are used for CFO estimation while (as before) 1, 5, or 9 out of the ten pilot slots are used for I/Q imbalance compensation. In general, the CFO estimates are used in the receivers for derotation, after which the receiver signal processing proceeds as earlier (diversity combining and I/Q imbalance estimation-compensation). The results are shown in Fig. 12, evidencing reliable overall operation with the given CFO estimation principle included. Overall, this demonstrates that the proposed principles can provide good compensation performance under very realistic signaling assumptions. For other recent work on CFO estimation and I/Q imbalances in general, refer to [37] and the references therein.

VI. Conclusion

This paper addressed the I/Q imbalance problem in multiantenna space-time transmit diversity (STTD) communication systems. Analytic signal models were derived describing the exact effect of I/Q imbalance on the overall system data transmission in closed-form. Based on these models, the resulting signal degradation due to I/Q imbalance was analyzed analytically in terms of the signal-to-interference ratio (SIR) at the combiner output. In general, the analysis shows that the analog front-end non-idealities play even more critical and complicated role in multiantenna systems than in their more traditional single-antenna counterparts, and needs to be fully

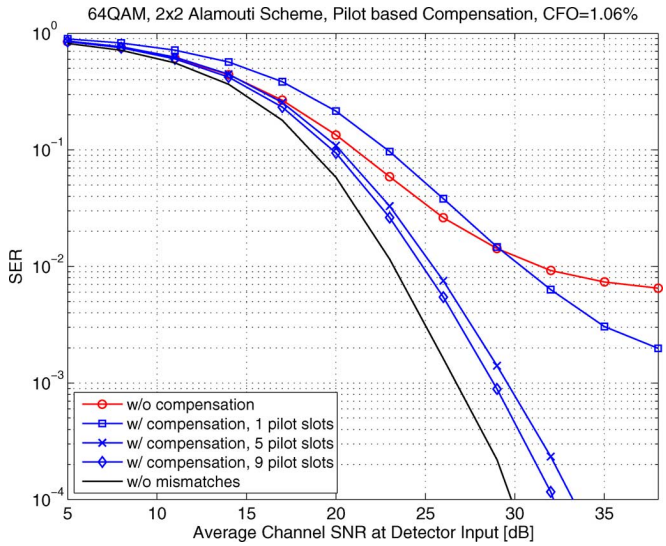

Fig. 12. Average symbol error rate (SER) performance of the pilot based imbalance compensator with $\sim 1\%$ carrier frequency offset in the receiver, including also CFO estimation. Perfectly matched reference is also shown assuming no I/Q imbalances and perfect synchronization.

appreciated in the future system and terminal equipment design. In addition to signal analysis, some novel DSP-based compensation techniques for mitigating the I/Q imbalance effects were also proposed. The first proposed scheme stems from pilot or training data-based estimation-correction principle while the second proposed technique builds on blind signal separation principles combined with proper I/Q decomposition of the received signal. Both schemes were shown to provide compensation performance close to or practically at the AWGN bound under rather realistic signaling assumptions, without affecting the overall diversity gain of the STTD principle. It was further shown that the proposed compensators are also, by design, able to correct for the channel estimation inaccuracies in addition to I/Q impairments, and are also reasonably robust against residual carrier offsets. Future work will be devoted to extending the presented analysis and compensation developments to more challenging propagation environments and frequency-selective I/Q imbalances. Also extending the work towards MIMO-OFDM type systems offers an interesting and important topic for future studies.

ACKNOWLEDGMENT

The authors would like to thank Prof. V. Koivunen, Helsinki University of Technology, Finland, for fruitful discussions and technical guidance. The authors would also like to thank the anonymous reviewers for their careful reviews, and for the comments and suggestions that helped them to considerably improve the contents and quality of the paper.

REFERENCES

[1] R. Tafazolli, Ed., Technologies for the Wireless Future: Wireless World Research Forum (WWRF). Chichester, U.K., Wiley, 2004.
[2] H.-H. Chen and M. Guizani, "Multiple access technologies for B3G wireless communications," *IEEE Commun. Mag.*, vol. 43, no. 2, pp. 65–67, Feb. 2005.
[3] A. Paulraj, R. Nabar, and D. Gore, *Introduction to Space-Time Wireless Communications*. Cambridge, U.K.: Cambridge Univ. Press, 2003.
[4] D. Gesbert *et al.*, "From theory to practice: An overview of MIMO space-time coded wireless systems," *IEEE J. Sel. Areas Commun.*, vol. 21, no. 3, pp. 281–302, Apr. 2003.
[5] S. M. Alamouti, "A simple transmit diversity technique for wireless communications," *IEEE J. Sel. Areas Commun.*, vol. 16, no. 8, pp. 1451–1458, Oct. 1998.
[6] *User Equipment (UE) Radio Transmission and Reception (FDD)," Technical Specification*, 3GPP Technical Specification Group Radio Access Network TS 25.101, V7.2.0, 2005.
[7] X. Li and M. Ismail, *Multi-Standard CMOS Wireless Receivers*. Norwell, MA: Kluwer, 2002.
[8] C. Chien, *Digital Radio Systems on a Chip*. Norwell, MA: Kluwer, 2001.
[9] W. Tuttlebee, Ed., *Software Defined Radio: Enabling Technologies*. Chichester, U.K.: Wiley, 2002.
[10] P. Kenington, *RF and Baseband Techniques for Software Defined Radio*. Norwood, MA: Artech House, 2005.
[11] M. Valkama, J. Pirskanen, and M. Renfors, "Signal processing challenges for applying software radio principles in future wireless terminals: An overview," *Int. J. Commun. Syst.*, vol. 15, pp. 741–769, Oct. 2002.
[12] S. Mirabbasi and K. Martin, "Classical and modern receiver architectures," *IEEE Commun. Mag.*, vol. 38, no. 11, pp. 132–139, Nov. 2000.
[13] B. Razavi, *RF Microelectronics*. Upper Saddle River, NJ: Prentice-Hall, 1998.
[14] B. Razavi, "Design considerations for direct-conversion receivers," *IEEE Trans. Circuits Syst. II*, vol. 44, pp. 428–435, Jun. 1997.
[15] A. Abidi, "Direct-conversion radio transceivers for digital communications," *IEEE J. Solid-State Circuits*, vol. 30, pp. 1399–1410, Dec. 1995.
[16] J. Crols and M. S. J. Steyaert, *CMOS Wireless Transceiver Design*. Dordrecht, The Netherlands: Kluwer, 1997.
[17] M. Valkama, "Advanced I/Q signal processing for wideband receivers: Models and algorithms," Ph.D. dissertation, Tampere University of Technology, Tampere, Finland, 2001.
[18] P. Rykaczewski, D. Pienkowski, R. Circa, and B. Steinke, "Signal path optimization in software defined radio systems," *IEEE Trans. Microw. Theory Tech.*, vol. 53, pp. 1056–1064, Mar. 2005.
[19] I.-H. Sohn, E.-R. Jeong, and Y. H. Lee, "Data-aided approach to I/Q mismatch and dc-offset compensation in communication receivers," *IEEE Commun. Lett.*, vol. 6, pp. 547–549, Dec. 2002.
[20] M. Valkama and M. Renfors, "Digital I/Q imbalance compensation in direct-conversion receivers," in *Proc. 2002 Workshop on Software Radios*, Karlsruhe, Germany, Mar. 2002, pp. 51–55.
[21] M. Valkama, M. Renfors, and V. Koivunen, "Blind I/Q signal separation-based solutions for receiver signal processing," *EURASIP J. Appl. Signal Process. (Special Issue on DSP Enabled Radios)*, vol. 2005, no. 16, pp. 2708–2718, Sep. 2005.
[22] G. Fettweis *et al.*, "Dirty RF," in *Proc. Wireless World Research Forum (WWRF) Meeting*, Oslo, Norway, Jun. 2004, vol. 11.
[23] M. Valkama, Y. Zou, and M. Renfors, "On I/Q imbalance effects in MIMO space-time coded transmission systems," in *Proc. IEEE Radio Wireless Symp. (RWS'06)*, San Diego, CA, Jan. 2006, pp. 223–226.
[24] J. Liu *et al.*, "Impact of front-end effects on the performance of downlink OFDM-MIMO transmission," in *Proc. IEEE Radio Wireless Conf. (RAWCON'04)*, Atlanta, GA, Sep. 2004, pp. 159–162.
[25] R. M. Rao and B. Daneshrad, "I/Q mismatch cancellation for MIMO-OFDM systems," in *Proc. IEEE Int. Symp. Pers., Indoor, Mobile Radio Commun. (PIMRC'04)*, Barcelona, Spain, Sep. 2004, pp. 2710–2714.
[26] T. C. W. Schenk, P. F. M. Smulders, and E. R. Fledderus, "Estimation and compensation of TX and RX IQ imbalance in OFDM-based MIMO systems," in *Proc. IEEE Radio Wireless Conf. (RAWCON'06)*, San Diego, CA, Jan. 2006, pp. 215–218.
[27] H. Kamata, K. Sakaguchi, and K. Araki, "An effective IQ imbalance compensation scheme for MIMO-OFDM communication system," presented at the IEEE Int. Symp. Pers., Indoor, Mobile Radio Commun. (PIMRC'05), Berlin, Germany, Sep. 2005.
[28] A. Tarighat and A. H. Sayed, "MIMO OFDM receivers for systems with IQ imbalances," *IEEE Trans. Signal Process.*, vol. 53, no. 9, pp. 3583–3596, Sep. 2005.
[29] T. C. W. Schenk, P. F. M. Smulders, and E. R. Fledderus, "Estimation and compensation of frequency selective TX/RX IQ imbalance in MIMO OFDM systems," in *Proc. IEEE Int. Conf. Communications (ICC'06)*, Istanbul, Turkey, Jun. 2006, pp. 251–256.
[30] P. J. Schreier and L. L. Scharf, "Second-order analysis of improper complex random vectors and processes," *IEEE Trans. Signal Process.*, vol. 51, no. 3, pp. 714–725, Mar. 2003.

[31] S. Haykin, Ed., *Unsupervised Adaptive Filtering, Vol. I: Blind Source Separation*. New York: Wiley, 2000.
[32] J.-F. Cardoso, "Blind signal separation: Statistical principles," *Proc. IEEE*, vol. 86, pp. 2009–2025, Oct. 1998.
[33] J.-F. Cardoso and B. H. Laheld, "Equivariant adaptive source separation," *IEEE Trans. Signal Process.*, vol. 44, no. 12, pp. 3017–3030, Dec. 1996.
[34] L. He, T. Thaiupathump, and S. A. Kassam, "Blind separation of complex I/Q independent sources with phase recovery," *IEEE Signal Process. Lett.*, vol. 12, no. 5, pp. 419–422, May 2005.
[35] E. A. Lee and D. G. Messerschmitt, *Digital Communication*, 2nd ed. Norwell, MA: Kluwer, 1994.
[36] S. Haykin, *Adaptive Filter Theory*, 3rd ed. Upper Saddle River, NJ: Prentice-Hall, 1996.
[37] S. dde Rore, "Joint estimation of carrier frequency offset and IQ imbalance for 4G mobile wireless systems," in *Proc. IEEE Int. Conf. Communications (ICC'06)*, Istanbul, Turkey, Jun. 2006, pp. 2066–2071.

Yaning Zou (S'05) was born in Chengdu, China, on September 21, 1980. She received the Bachelor's degree in communications engineering from the University Electronic Science and Technology of China (UESTC), Chengdu, China, in 2002, and the M.Sc. degree in electrical engineering from Tampere University of Technology (TUT), Tampere, Finland, in 2005.

Currently, she is working as a researcher and working towards the Ph.D. degree with the institute of communications engineering at TUT, Finland. Her general research interests are in signal processing algorithms for software defined flexible radios, and particularly in MIMO transceiver design.

Mikko Valkama (S'00–M'02) was born in Pirkkala, Finland, on November 27, 1975. He received the M.Sc. and Ph.D. degrees (both with honors) in electrical engineering from Tampere University of Technology (TUT), Finland, in 2000 and 2001, respectively.

In 2003, he was working as a visiting researcher with the Communications Systems and Signal Processing Institute at San Diego State University (SDSU), San Diego, CA. Currently, he is working as a senior researcher with the Institute of Communications Engineering at TUT, Finland. His general research interests include communications signal processing, estimation and detection techniques, signal processing algorithms for software defined flexible radios, and digital transmission techniques such as different variants of multicarrier modulation methods and OFDM.

Dr. Valkama has been involved in organizing IEEE conferences, such as the IEEE Workshop Signal Processing Advances Wireless Communications (SPAWC) 2007, held in Helsinki, Finland, for which he was Publications Chair. In 2002, he received the Best Ph.D. Thesis Award by the Finnish Academy of Science and Letters for his thesis titled "Advanced I/Q Signal Processing for Wideband Receivers: Models and Algorithms."

Markku Renfors (S'77–M'82–SM'90–F'08) was born in Suoniemi, Finland, on January 21, 1953. He received the Diploma Engineer, Licentiate of Technology, and Doctor of Technology degrees from Tampere University of Technology (TUT), Finland, in 1978, 1981, and 1982, respectively.

He held various research and teaching positions at TUT from 1976 to 1988. From 1988 to 1991, he was working as a Design Manager in the area of video signal processing, especially for HDTV, at Nokia Research Centre and Nokia Consumer Electronics. Since 1992, he has been a Professor and Head of the Institute of Communications Engineering at TUT. His main research areas are multicarrier systems and signal processing algorithms for flexible radio receivers and transmitters.

Dr. Renfors has been involved in the organization of the International Symposium on Circuits and Systems (ISCAS) 1988 as Symposium Committee Secretary; the International Conference on Communications (ICC) 2001 as Technical Program Vice-Chair, Tutorials; the Personal, Indoor Mobile Radio Communications Conference (PIMRC) 2006 as Technical Program Vice-Chair, Tutorials; and the IEEE Workshop Signal Processing Advances Wireless Communications (SPAWC) 2007 as Technical Program Co-Chair.